Article

Correlation between Key Steps and Hydricity in CO$_2$ Hydrogenation Catalysed by Non-Noble Metal PNP-Pincer Complexes

Snehasis Moni and Bhaskar Mondal *

School of Chemical Sciences, Indian Institute of Technology Mandi, Mandi 175005, Himachal Pradesh, India
* Correspondence: bhaskarmondal@iitmandi.ac.in

Abstract: Transition metal-catalysed homogeneous hydrogenation of CO$_2$ to formate or formic acid has emerged as an appealing strategy for the reduction of CO$_2$ into value-added chemicals. Since the state-of-the-art catalysts in this realm are primarily based on expensive precious metals and require demanding reaction conditions, the design and development of economically viable non-noble metal catalysts are in great demand. Herein, we exploit the thermodynamic correlation between the crucial reaction steps of CO$_2$ hydrogenation, that is, base-promoted H$_2$-splitting and hydride transfer to CO$_2$ as a guide to estimate the catalytic efficiency of non-noble metal complexes possessing a ligand backbone containing a secondary amine as an "internal base". A set of three non-noble metal complexes, one bearing tri-coordinated PNP-pincer (**1$_{Mn}$**) and the other two based on tetra-coordinated PNPN-pincer (**2$_{Mn}$** and **3$_{Fe}$**), have been investigated in this study. The computational mechanistic investigation establishes the role of the "internal" amine base in heterolytically splitting the metal-bound H$_2$, a critical step for CO$_2$ hydrogenation. Furthermore, the thermodynamic correlation between the hydricity ($\Delta G^{\circ}_{H^-}$) of the in situ generated metal-hydride species and the free energy barrier of the two crucial steps could provide an optimal hydricity value for efficient catalytic activity. Based on the computational estimation of the optimal hydricity value, the tri-coordinated PNP-pincer complex **1$_{Mn}$** appears to be the most efficient among the three, with the other two tetra-coordinated PNPN-pincer complexes, **2$_{Mn}$** and **3$_{Fe}$**, showing promising hydricity values. Overall, this study demonstrates how the crucial thermodynamic and kinetic parameters for pincer-based complexes possessing an "internal base" can be correlated for the prediction of novel non-noble metal-based catalysts for CO$_2$ hydrogenation.

Keywords: CO$_2$ hydrogenation; non-noble metal; PNP pincer ligand; internal base; hydricity; DFT calculations

1. Introduction

The anthropogenic release of CO$_2$ due to the extensive combustion of fossil fuels creates environmental turmoil [1,2]. Over the past few decades, the drastic increase in atmospheric CO$_2$ concentration has triggered climate change, global warming, rising sea levels, ocean acidification, etc. [3–6] This motivates researchers to search for alternative fuels and renewable energy sources. In this direction, the utilization of CO$_2$ as a C1 source for value-added chemicals and fuels has attracted significant research attention in recent times owing to the low-cost, high abundance, relatively low toxicity, and recyclability of CO$_2$ [7,8]. Over the past twenty years, economically viable strategies have been developed through which atmospheric CO$_2$ can be converted into environmentally congenial fuel components [9,10]. However, the reduction of CO$_2$ poses tremendous challenges due to its thermodynamic stability and kinetic inertness [11]. The kinetic inertness of CO$_2$ demands efficient catalytic processes, which usually involve multiple-electron transfer coupled with protons or Lewis acids (e.g., transition metals) [9–11]. In this direction, a great amount of research has been devoted to developing both homogeneous and heterogeneous catalytic processes for converting CO$_2$ to useful chemicals and fuels [12,13].

Among the wide variety of homogeneous CO_2 reduction pathways [7,14–16], CO_2 hydrogenation becomes one of the most attractive ones as this pathway can offer a myriad range of value-added chemicals, such as formic acid, formate, formaldehyde, methanol, methane, etc. [17–19], and can serve as a crucial step for sustainable organic syntheses [20,21]. The elemental CO_2 hydrogenation process leading to formic acid, formate, or their derivatives is particularly one of the most efficient pathways of CO_2 conversion to useful chemicals [22–26]. Since the first report of homogeneous CO_2 hydrogenation by Inoue et al. [27], an appreciable number of noble and non-noble transition metal-based homogeneous CO_2 hydrogenation catalysts have been reported with noteworthy turnover numbers (TON) and turnover frequencies (TOF) [9,26]. Among the noble metal catalysts, an iridium-pincer catalyst [IrH$_3$(PNP^{i}Pr)] (PNP^{i}Pr = 2,6-(CH$_2$P^{i}Pr$_2$)$_2$C$_5$H$_3$N) was reported to exhibit a remarkable highest-to-date TOF of 150,000 h^{-1} for CO_2 hydrogenation to formate [28]. However, when it comes to the non-noble metal catalysts, the reactivity lacks far behind that of noble metals. The highest CO_2 hydrogenation reactivity with a TOF of 74,000 h^{-1} has been reported with a cobalt(I)-phosphine catalyst, [Co^I(dmpe)$_2$H] (dmpe = 1,2-bis(dimethylphosphino)ethane), in the presence of a very strong Verkade base [29]. Therefore, it is highly desirable to develop robust CO_2 hydrogenation catalysts based on environmentally benign and cost-effective non-noble metals that can operate in ambient conditions. The rational design and development of such catalysts necessitate an atomic-level, understating of the key reaction steps of CO_2 hydrogenation and crucial thermodynamic and kinetic factor(s) that dictate the overall reactivity.

Transition metal-catalyzed CO_2 hydrogenation usually follows a common reaction mechanism as shown in Scheme 1a [30]. The catalytic cycle consists of three distinct reactions steps, involving (i) base-promoted H$_2$-splitting to form a metal hydride species (**I1** → **I2**), (ii) nucleophilic attack of hydride (H$^-$) of the metal-hydride species (**I2**) undergoing hydride transfer from metal to CO_2 (**I3** → **I4**), and (iii) protonation of the terminal oxygen of formate (HCOO$^-$) and release of the formic acid (**I4** → **I5**). Previous reports showed that among these three steps, either H$_2$-splitting or hydride transfer can act as the rate-determining step (RDS) of the entire catalytic cycle depending on the nature of the catalyst and the corresponding metal-hydride complex [30–34]. This catalyst-dependent switching of the RDS was demonstrated experimentally using Ru(II) [(η^6-C$_6$Me$_6$)-Ru^{II}(bpy)(H)]$^+$ and Ir(III) [(η^5-C$_5$Me$_5$)Ir^{III}(bpy)-(H)]$^+$ (bpy = 2,2′-bipyridine) complexes, where the former exhibited an H$_2$-splitting RDS and the later showed a hydride transfer RDS [35].
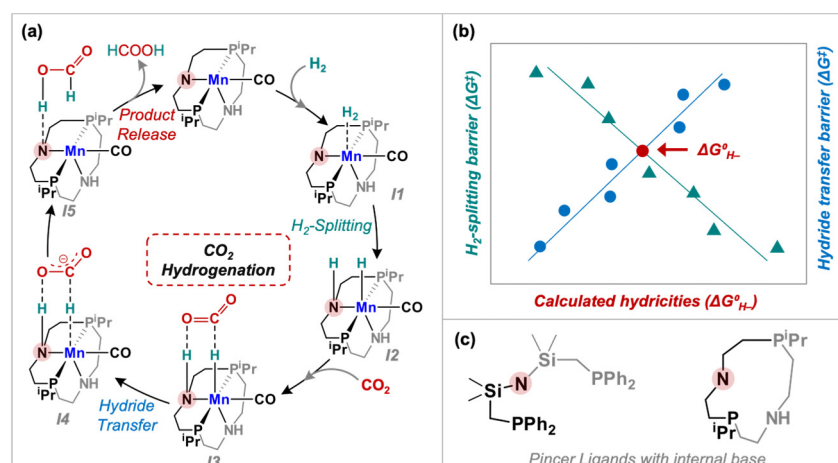

Scheme 1. (**a**) Established reaction mechanism and steps involved in homogeneous CO_2 hydrogenation. (**b**) Schematic representation of the correlation diagram between the two key reaction steps of CO_2 hydrogenation and hydricity. (**c**) Chemical structures of the tri- and tetra-coordinated pincer ligands.

It has been realized that the H_2-splitting step is driven by the strength of the M–H bond formation in the metal hydride; on the other hand, the hydride transfer is driven by the ability of the M–H bond to donate the H^- to CO_2 [36,37]. As such, the electronic requirement of the two key steps is quite the opposite. Therefore, a delicate balance must be maintained between the two key steps of CO_2 hydrogenation, that is, H_2 splitting and hydride transfer for efficient execution of the reaction. As the two crucial steps are connected by the intermediacy of the M–H bond in the metal hydride intermediate (**I2**), the balance is controlled by the strength of the M–H bond (Scheme 1b). The M–H bond strength can be quantified using a thermodynamic parameter, called hydricity ($\Delta G^\circ_{H^-}$), which is a measure of the ability of the metal-hydride complex to donate its hydride. Understandably, a lower hydricity (less positive value) will ease the hydride donation, and the opposite is true for the H_2 splitting process. Using phosphine-based catalysts of the type $[M(H)(\eta^2\text{-}H_2)(PP_3^{Ph})]^{n+}$ (M = Fe(II), Ru(II), and Co(III); PP_3^{Ph} = *tris*(2-(diphenylphosphino)phenyl)phosphine), Mondal et al. established that metal hydride species possessing relatively low hydricity exhibit base-promoted H_2-splitting RDS, whereas complexes with high hydricity undergo hydride transfer RDS [36]. In a subsequent report, the same group used hydricity as a guide to present rational design strategies for predicting efficient CO_2 hydrogenation catalysts based on non-noble metals [37]. These computational reports have been truly motivating in the rational design and development of non-noble metal-based catalysts for CO_2 hydrogenation to formate or formic acid.

One of the major challenges in base-assisted CO_2 hydrogenation reactions is the requirement of an "external" sacrificial base to promote the H_2-splitting step as well as the product release. This can be efficiently circumvented using pincer-based complexes featuring an "internal base" in-built into the pincer ligand. Leitner and coworkers reported how metal-ligand cooperation through a secondary amine (–N–) functionality in the Mn-PNP pincer complex (1_{Mn}) can promote the activation of pinacolborane during the hydroboration of carbon dioxide [38]. Later on, a computational mechanistic investigation by Lei and coworkers demonstrated the promising potential of complex 1_{Mn} towards CO_2 hydrogenation to methanol [39]. Hazari et al. showcased how the Lewis acidic behavior of a PNP-pincer ligand's N–H moiety can be exploited for the Fe-catalyzed CO_2 hydrogenation to formate [40]. A similar Fe-pincer catalytic system was also used by Bernskoetter et al. for the CO_2 hydrogenation to methanol [41]. These reports present a highly promising prospect that the N-atom in the pincer chain (Scheme 1c) can be exploited as a base for the crucial H_2-splitting step and the corresponding form as a Lewis acid to stabilize the formate product (Scheme 1a). The tri-coordinated PNP-pincer ligands, although extremely efficient in inducing versatile catalytic reactivities in transition metal complexes, occasionally suffer from ligand dissociation in harsh reaction conditions. Very recently, Li et al. computationally predicted that a more rigid version of the pincer ligand, tetra-coordinated PNPN pincer (Scheme 1c), can be highly promising in the hydrogenolysis of polyurethanes [42]. The computationally predicted novel Mn- and Fe-based tetra-coordinated PNPN complexes (2_{Mn} and 3_{Fe}) possessing an "internal base" appear highly promising toward CO_2 hydrogenation.

Herein, we investigate how the two crucial reaction steps of CO_2 hydrogenation to formate/formic acid are the base-promoted H_2-splitting and hydride transfer in the catalytic cycle of metal-pincer complexes featuring an "internal base" are correlated with the hydricity of the metal-hydride intermediate. Specifically, we have performed a mechanistic investigation and reaction energetics calculations on the tetra-coordinated PNPN-pincer complexes 2_{Mn} and 3_{Fe} along with the experimentally reported tri-coordinated Mn-PNP pincer complex 1_{Mn} (Scheme 2) using density functional theory (DFT) calculations. Importantly, we have correlated the driving force (ΔG) and reaction barrier ($\Delta G^\ddagger$) of the H_2-splitting and hydride transfer steps of all the complexes (**1–3**) with the calculated hydricities of their metal-hydride intermediates. Finally, based on the correlation plots, we predicted the catalytic potential of the non-noble metal PNP-pincer complexes for CO_2 hydrogenation.
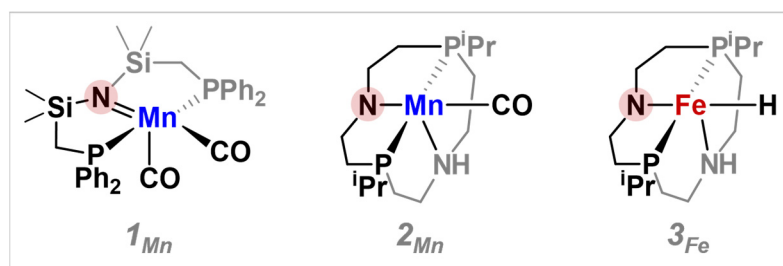
Scheme 2. PNP-pincer complexes (**1–3**) of the non-noble metals (Mn and Fe) possessing the N-atom as an "internal base" are investigated in this work.

2. Computational Details

All the geometry optimizations and harmonic vibrational frequency calculations have been performed at the density functional theory (DFT) level, employing the range-separated hybrid functional ωB97XD in conjunction with the LANL2DZ basis set and corresponding effective core potential (ECP) on the metals and Pople's double-ξ basis set 6-31G(d,p) on the main-group elements. The conductor-like continuum solvation model (CPCM) with tetrahydrofuran (THF, $\varepsilon = 7.4257$) as solvent was employed during the geometry optimization. We also investigated whether there is any explicit solvent effect on the intrinsic reaction barrier and driving force using an explicit solvent (THF) molecule in the proximity of the reaction center. No noticeable change in the barrier and the driving force was observed due to the explicit solvent molecule (Figure S1 from Supplementary Materials). For a relatively accurate estimation of reaction energetics, a basis set combination of LANL2TZ and the corresponding ECP on the metals and the triple-ξ basis set 6-311++G(d,p) describing the main-group elements was used for the calculation of electronic energies at the ωB97XD level. The long-range corrected DFT functional ωB97XD has been reported in the literature to produce reliable results on the reaction energetics of metal-pincer complexes [32]. All the transition states were confirmed by connecting the reactants and products by intrinsic reaction coordinate (IRC) calculations and characterized by only one imaginary frequency. The enthalpies (H) and Gibbs free energies (G) were calculated at standard conditions, 298 K and 1 atm. All the calculations were performed using the Gaussian 16 suite of the quantum chemistry program [43]. A detailed description of the calculation of thermodynamic hydricities ($\Delta G^{\circ}_{H^-}$) [44–48] at the DFT level is presented in the Supporting Information.

3. Results and Discussion

The complete reaction free energy profile involving the reaction steps described in Scheme 1a for CO_2 hydrogenation catalyzed by the reported Mn(I)-PNP pincer complex **1$_{Mn}$** leading to formic acid is presented in Figure 1. The energetics for the different reaction steps is calculated at the DFT-ωB97xD level. Prior to the H_2-splitting, the molecular hydrogen binds to the Mn-center in an endergonic manner (**I1**, $\Delta G = 10.6$ kcal/mol) followed by the base-promoted splitting of the metal-bound H_2 to generate the metal-hydride intermediate (**I2**). The N-atom of the PNP-pincer ligand serves as the "internal base" to assist the H_2-splitting process. The overall process (**1$_{Mn}$** → **I2**) appears to be thermoneutral ($\Delta G = 0.1$ kcal/mol) and involves a moderate free-energy barrier of 14.6 kcal/mol through an H_2-splitting transition state (**TS1**). The net free energy barrier and free energy change for the H_2 splitting step are similar to that reported earlier by Lei et al. [39] Importantly, the intrinsic driving force, that is, from the metal-bound H_2 complex to the metal-hydride intermediate (**I1** → **I2**), is calculated to be 10.5 kcal/mol, and the corresponding free-energy barrier is only 4.0 kcal/mol (**I1** → **TS1**). The low intrinsic free energy barrier for the H_2-splitting step for **1$_{Mn}$** is due to the large entropic penalty associated with the H_2 binding, as clearly seen from the 4.7 kcal/mol overall enthalpy barrier. A relatively large intrinsic driving force for the H_2-splitting process (**I1** → **I2**) for **1$_{Mn}$** is indicative of a rather strong Mn–H bond in the metal-hydride intermediate **I2**.
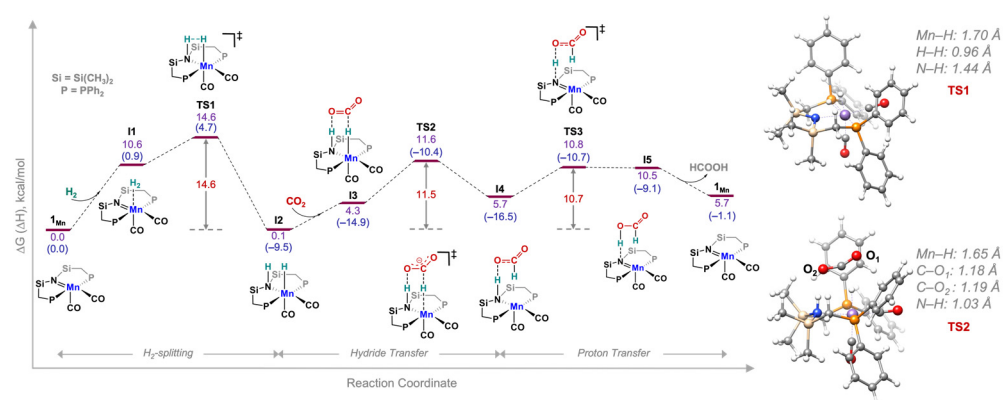
Figure 1. The free energy (ΔG in kcal/mol) profile along with the transition states of the key steps of CO_2 hydrogenation to formic acid catalyzed by ($\mathbf{1_{Mn}}$) at the ωB97XD/[6-311++G(d,p)+LANL2TZ]/ CPCM(THF) level of theory. Relative enthalpy (ΔH in kcal/mol) values are presented in parentheses. ‡ symbol is used to denote transition states.

A moderately endergonic binding of CO_2 (ΔG = 4.2 kcal/mol) to the metal hydride intermediate **I2** to form a CO_2 adduct **I3** precedes the hydride transfer step and the resulting intermediate **I3** undergoes hydride transfer to CO_2 to form a formate ($HCOO^-$)-bound intermediate **I4**. The overall free energy barrier for the hydride transfer step was calculated to be 11.5 kcal/mol (**I2** $\rightarrow$ **TS2**) with an intrinsic barrier of 7.3 kcal/mol (**I3** $\rightarrow$ **TS2**). The hydride transfer step for $\mathbf{1_{Mn}}$ was calculated to be overall endergonic by 5.7 kcal/mol and intrinsically thermoneutral (**I3** $\rightarrow$ **I4**, ΔG = 1.4 kcal/mol). Therefore, considering the intrinsic free energy barriers and driving forces, the H_2-splitting step appears to be energetically more feasible for $\mathbf{1_{Mn}}$ as compared to the hydride transfer step.

The final step, involving a proton transfer from the "internal base", i.e., the N-atom of the PNP-pincer ligand to the formate ($HCOO^-$), leads to the formic acid-bound catalyst complex (**I5**) through an endergonic process (**I4** $\rightarrow$ **I5**, ΔG = 4.8 kcal/mol). This proton transfer step involves an intrinsic barrier of 5.1 kcal/mol and an overall barrier of 10.7 kcal/mol. The final release of formic acid (HCOOH) and catalyst regeneration (**I5** $\rightarrow$ $\mathbf{1_{Mn}}$) makes the overall process thermoneutral.

As evident from the overall free energy profile in Figure 1 for the CO_2 hydrogenation reaction catalyzed by $\mathbf{1_{Mn}}$, base-promoted H_2-splitting appears to be the rate-determining step of the overall catalytic cycle. This result is consistent with the previous literature reports on the CO_2 hydrogenation reaction catalyzed by metal-pincer complexes (M = Ir, Fe, Co, Mn) [32,39]. As our main focus remains on the correlation between the free energy barrier of the key steps and the hydricity of the metal-hydride intermediate, a fair comparison between different catalysts needs reaction barriers to be ascertained on the basis of an identical reference point. To this end, calculation of the free energy barrier using the infinitely separated species (catalyst + H_2) typically predict a substantial entropy change of ~10 kcal/mol due to the loss of translational and rotational degrees of freedom, as was also observed for the three catalysts under investigation [36,37,49]. Therefore, we use the reaction barrier for the key steps, the intrinsic barrier, using the reactant complex (**I1**) as the reference point for all the catalysts $\mathbf{1_{Mn}}$, $\mathbf{2_{Mn}}$, and $\mathbf{3_{Fe}}$. A similar strategy of using such "intrinsic barriers" to establish the correlation between the key steps and hydricity in CO_2 hydrogenation reactions has been reported in the literature [36,37].

After analyzing the key steps' energetics for the reported Mn-PNP complex, we investigated the same for the computationally predicted tetra-coordinated PNPN-pincer complexes of Mn ($\mathbf{2_{Mn}}$) and Fe ($\mathbf{3_{Fe}}$). We particularly focus on the reaction energetics of the two key steps only, i.e., base-promoted H_2-splitting, and hydride transfer in the following discussion. Figure 2 represents the reaction energetics of the key steps exhibited by $\mathbf{2_{Mn}}$. The complex $\mathbf{2_{Mn}}$ inherits the lowest energy conformer, where the CO ligand coordinates to one of the tetragonal positions (Figure S2). The catalytically active form of $\mathbf{2_{Mn}}$ is calculated

to possess a triplet ground state (^{3}**2$_{Mn}$**, Figure 2) that is 4.6 kcal/mol lower in free energy as compared to the singlet. However, the triplet state (^{3}**2$_{Mn}$**) does not bind to the molecular hydrogen to undergo the crucial H_2-splitting process and must experience a triplet to singlet spin cross to perform the reaction. Such a spin cross can introduce some uncertainty in estimating the overall free energy barrier, which could be avoided through "intrinsic" free energy barriers. The singlet **2$_{Mn}$** experiences a thermoneutral H_2 binding to the Mn-center and, consequently, a moderately lower H_2-splitting free energy barrier of 8.4 kcal/mol (**I1** → **TS1**, Figure 2), leading to the metal-hydride intermediate **I2** through the H_2-splitting transition state **TS1**. This calculated free energy barrier is very similar to the earlier reported intrinsic H_2-splitting barrier [42]. The thermoneutral binding of the molecular H_2 to the Mn center of **2$_{Mn}$** may be attributed to the strong interaction between the Mn center and H_2, as evident from the appreciably high binding enthalpy of −6.8 kcal/mol. The overall H_2-splitting process has a thermodynamic driving force of 6.2 kcal/mol in terms of free energy. Unlike the H_2 binding, the binding of CO_2 to the Mn-hydride intermediate in the subsequent step is moderately endergonic by 5.7 kcal/mol, which is due to the relatively weak adduct between the metal-hydride intermediate **I2** and CO_2. The overall hydride transfer barrier is only 7.4 kcal/mol, including the CO_2 binding step, which implies a marginally low intrinsic hydride transfer barrier (1.7 kcal/mol) for the process. The net hydride transfer process is calculated to be highly exergonic by 8.5 kcal/mol (**I2** → **I4**) with an intrinsic driving force of 14.2 kcal/mol.
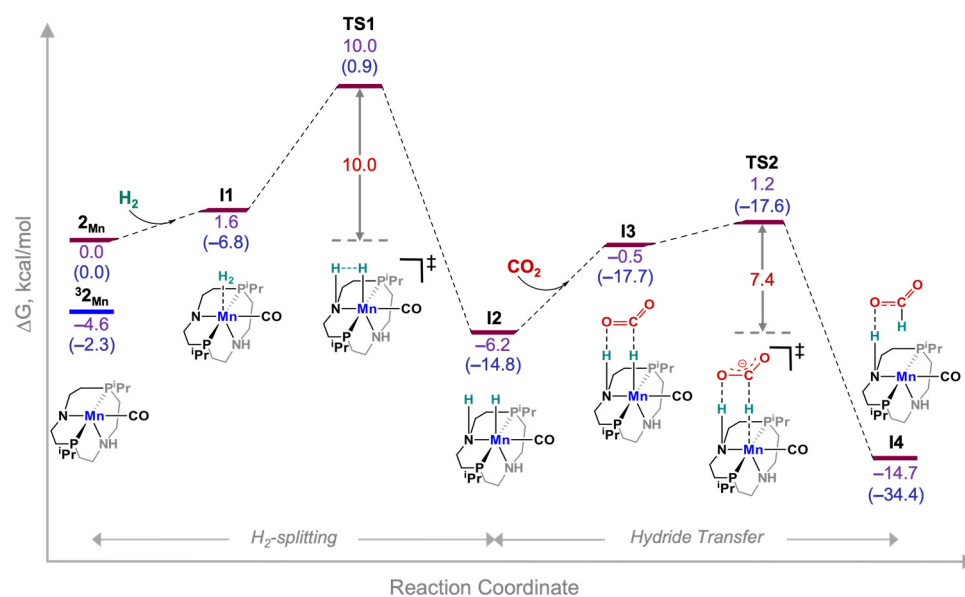
Figure 2. The free energy profile for the two key steps of CO_2 hydrogenation to formic acid catalyzed by complex **2$_{Mn}$** obtained at the ωB97XD/[6-311++G(d,p)+LANL2TZ]/CPCM(THF) level of theory. ‡ symbol is used to denote transition states.

Similar to complex **2$_{Mn}$**, **3$_{Fe}$** is a tetra-coordinated PNPN-pincer complex that was also theoretically predicted during the investigation of the hydrogenolysis of polyurethanes [42]. Complex **3$_{Fe}$** possesses the lowest energy conformer, where the H ligand coordinates to one of the tetragonal positions (Figure S2). Similar to complex **2$_{Mn}$**, the coordinatively unsaturated catalytically active form of **3$_{Fe}$** possesses a triplet ground state (^{3}**3$_{Fe}$**, Figure 3) that also does not bind to the molecular H_2. Therefore, the intrinsic reaction barriers for the key steps are obtained using singlet species. **3$_{Fe}$** undergoes H_2-splitting with an overall free energy barrier of 9.9 kcal/mol, which is similar to that of its Mn congener. The intrinsic barrier for this step for **3$_{Fe}$** appears to be just 2.5 kcal/mol lower, 7.4 kcal/mol (**I1** → **TS1**), as compared to the overall barrier. The subsequent hydride transfer step (**I2** → **TS2**) for **3$_{Fe}$** involves a lower barrier of 8.1 kcal/mol with a negligible intrinsic barrier of 2.0 kcal/mol

(**I3 → TS2**). Both the H_2-splitting and hydride transfer steps were calculated to have appreciable intrinsic driving forces of 10.4 and 13.9 kcal/mol, respectively.
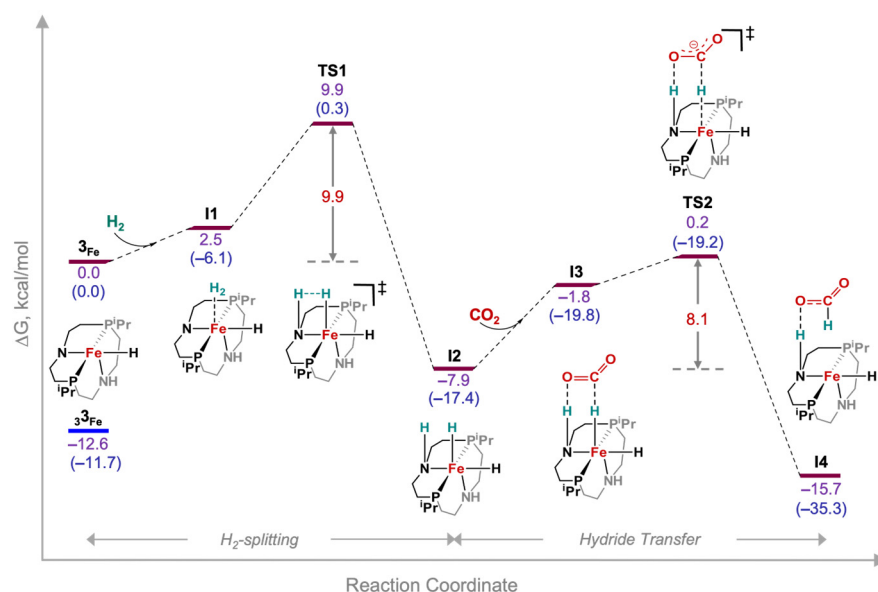
Figure 3. The free energy profile for the two key steps of CO_2 hydrogenation to formic acid catalyzed by complex $\mathbf{3_{Fe}}$ obtained at the ωB97XD/[6-311++G(d,p)+LANL2TZ]/CPCM(THF) level of theory. ‡ symbol is used to denote transition states.
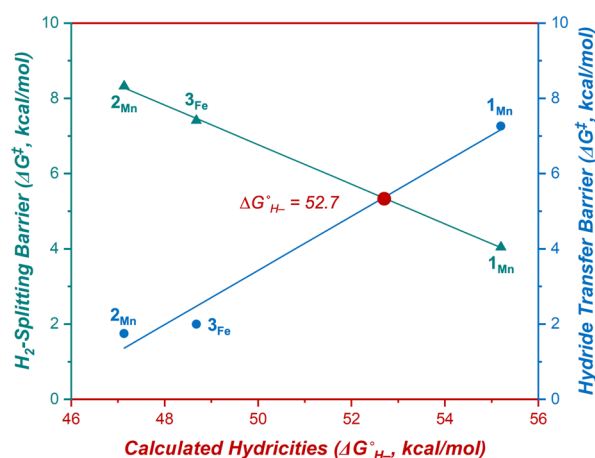
As reported earlier, the two key steps of CO_2 hydrogenation, which are base-promoted H_2-splitting and hydride transfer to CO_2 have opposite electronic requirements [30,36,37]. The metal-hydride intermediate (**I2**) is the bridge and helps attain the balance between the two steps through the M–H bond. The strength of the M–H bond is quantified by the thermodynamic parameter, hydricity ($\Delta G^{\circ}_{H^-}$), measuring the metal-hydride intermediate to donate its hydride. Therefore, correlations between the hydricity of **I2** and the free energy barrier of H_2-splitting and hydride transfer would regulate the efficiency of a catalyst towards CO_2 hydrogenation. To estimate the catalytic potential of complexes $\mathbf{1_{Mn}}$, $\mathbf{2_{Mn}}$, and $\mathbf{3_{Fe}}$, we correlated the calculated hydricities of their in situ generated metal-hydride intermediates (**I2**) with the corresponding barriers of H_2-splitting and hydride transfer. The computational protocol for calculating the hydricity is described in the Supporting Information. The computed hydricity of $HCOO^-$ matches exactly with the experimental value of 43.0 kcal/mol, which supports the computational method applied for calculating the hydricity in this work. Using the computational method of hydricity calculation as described in the Supporting Information, the calculated hydricities of $\mathbf{1_{Mn}}$, $\mathbf{2_{Mn}}$, and $\mathbf{3_{Fe}}$ are 55.2, 47.1, and 48.7 kcal/mol, respectively.

Earlier reports by Mondal et al. [36,37] on phosphine-based CO_2 hydrogenation catalysts clearly demonstrated that the calculated $\Delta G^{\circ}_{H^-}$ of the metal-hydride species is linearly well-correlated with the barriers ($\Delta G^{\ddagger}$) of both H_2-splitting and hydride transfer. As one can expect, $\Delta G^{\circ}_{H^-}$ was found to be negatively and positively correlated with the barriers of H_2-splitting and hydride transfer, respectively. This corroborates well with the opposite electronic requirements of the two key steps of CO_2 hydrogenation, that is, a stronger hydricity will promote the H_2 splitting step and a weaker hydricity will promote the hydride transfer step. However, the opposite electronic requirements of the two key steps are not appropriately reflected when we examine the correlation plots between the "overall" free energy barrier and calculated hydricity. Specifically, the H_2 splitting step shows an unexpected positive correlation (Figure S4a). On the other hand, the notion of the opposite electronic requirement of the two key steps of CO_2 hydrogenation is nicely followed for the current complexes when we consider the "intrinsic" free energy barrier. For instance, the complex $\mathbf{1_{Mn}}$ possessing the highest hydricity ($\Delta G^{\circ}_{H^-} = 55.2$ kcal/mol) among three

exhibits a very low intrinsic barrier for the H_2-splitting (4.0 kcal/mol). Whereas, for the other two complexes, **2_{Mn}** and **3_{Fe}**, possessing a relatively lower hydricity, the Intrinsic H_2-splitting barrier is much higher, at 8.4 and 7.4 kcal/mol, respectively (Table 1). The opposite was found true for the hydride transfer steps for the three complexes. Complex **1_{Mn}**, with the highest hydricity, traverses a much higher intrinsic hydride transfer barrier (7.3 kcal/mol) as compared to complexes **2_{Mn}** and **3_{Fe}** (1.7 and 2.0 kcal/mol, respectively) (Table 1). We observed a negative correlation between $\Delta G^{\circ}_{H^-}$ and $\Delta G^{\ddagger}$ of H_2-splitting ($R^2 = 1.00$, Figure S5a), and a positive correlation between $\Delta G^{\circ}_{H^-}$ and $\Delta G^{\ddagger}$ of hydride transfer ($R^2 = 0.98$, Figure S5b) for complexes **1_{Mn}**, **2_{Mn}**, and **3_{Fe}**. Thus, the use of an intrinsic free energy barrier, as also suggested in the earlier reports on CO_2 hydrogenation in ref. [30,36,37], gives thermodynamic correlations appropriately reflecting the electronic requirements of the key reaction steps. On merging the correlations between calculated hydricities of the metal-hydride intermediate (**I2**) and free energy barriers for the H_2-splitting and hydride transfer together, we could obtain an optimal value in the hydricity ($\Delta G^{\circ}_{H^-}$) scale, at 52.7 kcal/mol, that the catalysts under investigation need to strike for an optimal CO_2 hydrogenation reactivity (Figure 4).

Table 1. Calculated hydricity and intrinsic barriers for H_2 splitting and the hydride transfer step.

Species	Calculated Hydricity ($\Delta G^{\circ}_{H^-}$, kcal/mol)	Intrinsic H_2-Splitting Barrier ($\Delta G^{\ddagger}$, kcal/mol)	Intrinsic Hydride Transfer Barrier ($\Delta G^{\ddagger}$, kcal/mol)
1_{Mn}	55.2	4.0	7.3
2_{Mn}	47.1	8.4	1.7
3_{Fe}	48.7	7.4	2.0

Figure 4. Correlation plot between the intrinsic free energy barrier of the key steps of CO_2 hydrogenation and calculated hydricities of the metal-hydride intermediates obtained at the DFT-ωB97xD level.

The combined correlation plot presented in Figure 4 delivers an estimation of the optimal value for hydricity for Mn- and Fe-based complexes possessing an "internal base" in the tri- or tetra-coordinated PNP-pincer ligand framework. The metal-hydride intermediate generated from the Mn-pincer complex **1_{Mn}** reported by Leitner et al. appears to possess a hydricity value (55.2 kcal/mol) closest to the optimal value (52.7 kcal/mol); therefore, it can be considered as the most promising CO_2 hydrogenation catalyst among the three metal-pincer complexes. The Mn- and Fe-based tetra-coordinated PNPN-pincer complexes **2_{Mn}** and **3_{Fe}** possess hydricities of 47.1 and 48.1 kcal/mol, respectively, which are about 5–6 kcal/mol off from the estimated optimum value. Considering the uncertainty limit of the DFT-predicted hydricity and reaction barriers, the new tetra-coordinated PNPN-pincer complexes appear promising in homogeneous CO_2 hydrogenation.

4. Conclusions and Outlook

Non-noble metal-based pincer complexes possessing secondary amine as an "internal base" have been explored for homogeneous CO_2 hydrogenation in this study. Tri-coordinated PNP-pincer complexes are well-known for CO_2 hydrogenation; however, their tetra-coordinated congeners need attention towards CO_2 hydrogenation. The current DFT-based mechanistic investigation and reaction energetics calculations on one tri-coordinated PNP-pincer Mn complex (**1$_{Mn}$**) and two tetra-coordinated PNPN-pincer complexes (**2$_{Mn}$** and **3$_{Fe}$**) reveal the crucial role of the secondary amine moiety in-built in the pincer backbone in the heterolytic H_2-splitting. The elegant correlation between the calculated hydricity of the metal-hydride intermediate and the free energy barrier of the crucial H_2-splitting and hydride transfer steps have been used to estimate the catalytic potential of the three pincer complexes. Specifically, the correlation plot provided an optimum value for hydricity, which is 52.7 kcal/mol. Indeed, the reported Mn-PNP complex **1$_{Mn}$** appears to be the most promising in terms of the balancing hydricity (55.2 kcal/mol) of the corresponding metal-hydride species. The other two tetra-coordinated PNPN-pincer complexes, **2$_{Mn}$** and **3$_{Fe}$**, with relatively lower hydricity of their metal-hydride species, can be considered as potential catalysts for CO_2 hydrogenation within the uncertainty limit of the DFT calculations. This study provides a foundation for exploring the catalytic potential of a wide range of metal-pincer complexes towards CO_2 hydrogenation and will certainly guide novel catalyst design and development in this direction.

References

1. Solomon, S.; Plattner, G.-K.; Knutti, R.; Friedlingstein, P. Irreversible Climate Change Due to Carbon Dioxide Emissions. *Proc. Natl. Acad. Sci. USA* **2009**, *106*, 1704–1709. [CrossRef] [PubMed]
2. Davis, S.J.; Caldeira, K.; Matthews, H.D. Future CO_2 Emissions and Climate Change from Existing Energy Infrastructure. *Science* **2010**, *329*, 1330–1333. [CrossRef]
3. Bach, W. Impact of Increasing Atmospheric CO_2 Concentrations on Global Climate: Potential Consequences and Corrective Measures. *Environ. Int.* **1979**, *2*, 215–228. [CrossRef]
4. Lüthi, D.; Le Floch, M.; Bereiter, B.; Blunier, T.; Barnola, J.M.; Siegenthaler, U.; Raynaud, D.; Jouzel, J.; Fischer, H.; Kawamura, K.; et al. High-Resolution Carbon Dioxide Concentration Record 650,000–800,000 Years before Present. *Nature* **2008**, *453*, 379–382. [CrossRef]
5. Penuelas, J.; Fernández-Martínez, M.; Vallicrosa, H.; Maspons, J.; Zuccarini, P.; Carnicer, J.; Sanders, T.G.M.; Krüger, I.; Obersteiner, M.; Janssens, I.A.; et al. Increasing Atmospheric CO_2 Concentrations Correlate with Declining Nutritional Status of European Forests. *Commun. Biol.* **2020**, *3*, 1–11. [CrossRef]
6. Dincer, I. Environmental Impacts of Energy. *Energy Policy* **1999**, *27*, 845–854. [CrossRef]

7. Aresta, M.; Dibenedetto, A.; Angelini, A. Catalysis for the Valorization of Exhaust Carbon: From CO₂ to Chemicals, Materials, and Fuels. Technological Use of CO₂. *Chem. Rev.* **2014**, *114*, 1709–1742. [CrossRef]

8. Xiaoding, X.; Moulijn, J.A. Mitigation of CO₂ by Chemical Conversion: Plausible Chemical Reactions and Promising Products. *Energy Fuels* **1996**, *10*, 305–325. [CrossRef]

9. Appel, A.M.; Bercaw, J.E.; Bocarsly, A.B.; Dobbek, H.; Dubois, D.L.; Dupuis, M.; Ferry, J.G.; Fujita, E.; Hille, R.; Kenis, P.J.A.; et al. Frontiers, Opportunities, and Challenges in Biochemical and Chemical Catalysis of CO₂ Fixation. *Chem. Rev.* **2013**, *113*, 6621–6658. [CrossRef] [PubMed]

10. Darensbourg, D.J. Chemistry of Carbon Dioxide Relevant to Its Utilization: A Personal Perspective. *Inorg. Chem.* **2010**, *49*, 10765–10780. [CrossRef]

11. Mondal, B.; Song, J.; Neese, F.; Ye, S. Bio-Inspired Mechanistic Insights into CO₂ Reduction. *Curr. Opin. Chem. Biol.* **2015**, *25*, 103–109. [CrossRef]

12. Grice, K.A. Carbon Dioxide Reduction with Homogenous Early Transition Metal Complexes: Opportunities and Challenges for Developing CO₂ Catalysis. *Coord. Chem. Rev.* **2017**, *336*, 78–95. [CrossRef]

13. Cokoja, M.; Bruckmeier, C.; Rieger, B.; Herrmann, W.A.; Kühn, F.E. Transformation of Carbon Dioxide with Homogeneous Transition-Metal Catalysts: A Molecular Solution to a Global Challenge? *Angew. Chem. Int. Ed.* **2011**, *50*, 8510–8537. [CrossRef]

14. Sakakura, T.; Choi, J.C.; Yasuda, H. Transformation of Carbon Dioxide. *Chem. Rev.* **2007**, *107*, 2365–2387. [CrossRef]

15. Riduan, S.N.; Zhang, Y. Recent Developments in Carbon Dioxide Utilization under Mild Conditions. *Dalton Trans.* **2010**, *39*, 3347–3357. [CrossRef]

16. Benson, E.E.; Kubiak, C.P.; Sathrum, A.J.; Smieja, J.M. Electrocatalytic and Homogeneous Approaches to Conversion of CO2 to Liquid Fuels. *Chem. Soc. Rev.* **2009**, *38*, 89–99. [CrossRef] [PubMed]

17. Wang, W.; Wang, S.; Ma, X.; Gong, J. Recent Advances in Catalytic Hydrogenation of Carbon Dioxide. *Chem. Soc. Rev.* **2011**, *40*, 3703–3727. [CrossRef] [PubMed]

18. Kar, S.; Kothandaraman, J.; Goeppert, A.; Prakash, G.K.S. Advances in Catalytic Homogeneous Hydrogenation of Carbon Dioxide to Methanol. *J. CO2 Util.* **2018**, *23*, 212–218. [CrossRef]

19. Sordakis, K.; Tang, C.; Vogt, L.K.; Junge, H.; Dyson, P.J.; Beller, M.; Laurenczy, G. Homogeneous Catalysis for Sustainable Hydrogen Storage in Formic Acid and Alcohols. *Chem. Rev.* **2018**, *118*, 372–433. [CrossRef] [PubMed]

20. Huang, K.; Sun, C.; Shi, Z. Transition-Metal-Catalyzed C–C Bond Formation through the Fixation of Carbon Dioxide. *Chem. Soc. Rev.* **2011**, *40*, 2435–2452. [CrossRef] [PubMed]

21. Liu, Q.; Wu, L.; Jackstell, R.; Beller, M. Using Carbon Dioxide as a Building Block in Organic Synthesis. *Nat. Commun.* **2015**, *6*, 1–15. [CrossRef]

22. Federsel, C.; Jackstell, R.; Beller, M. State-of-the-Art Catalysts for Hydrogenation of Carbon Dioxide. *Angew. Chem. Int. Ed.* **2010**, *49*, 6254–6257. [CrossRef] [PubMed]

23. Jessop, P.G.; Ikariya, T.; Noyori, R. Homogeneous Hydrogenation of Carbon Dioxide. *Chem. Rev.* **1995**, *95*, 259–272. [CrossRef]

24. Jessop, P.G.; Joó, F.; Tai, C.-C. Recent Advances in the Homogeneous Hydrogenation of Carbon Dioxide. *Coord. Chem. Rev.* **2004**, *248*, 2425–2442. [CrossRef]

25. Rohmann, K.; Kothe, J.; Haenel, M.W.; Englert, U.; Hölscher, M.; Leitner, W. Hydrogenation of CO 2 to Formic Acid with a Highly Active Ruthenium Acriphos Complex in DMSO and DMSO/Water. *Angew. Chem. Int. Ed.* **2016**, *55*, 8966–8969. [CrossRef] [PubMed]

26. Klankermayer, J.; Wesselbaum, S.; Beydoun, K.; Leitner, W. Selective Catalytic Synthesis Using the Combination of Carbon Dioxide and Hydrogen: Catalytic Chess at the Interface of Energy and Chemistry. *Angew. Chem. Int. Ed.* **2016**, *55*, 7296–7343. [CrossRef]

27. Inoue, Y.; Izumida, H.; Sasaki, Y.; Hashimoto, H. Catalytic Fixation of Carbon Dioxide to Formic Acid by Transition-Metal Complexes Under Mild Conditions. *Chem. Lett.* **1976**, *5*, 863–864. [CrossRef]

28. Tanaka, R.; Yamashita, M.; Nozaki, K. Catalytic Hydrogenation of Carbon Dioxide Using Ir(III)-Pincer Complexes. *J. Am. Chem. Soc.* **2009**, *131*, 14168–14169. [CrossRef] [PubMed]

29. Jeletic, M.S.; Mock, M.T.; Appel, A.M.; Linehan, J.C. A Cobalt-Based Catalyst for the Hydrogenation of CO₂ under Ambient Conditions. *J. Am. Chem. Soc.* **2013**, *135*, 11533–11536. [CrossRef] [PubMed]

30. Roy, L.; Mondal, B.; Ye, S. Computational Mechanistic Insights into Non-Noble-Metal-Catalysed CO₂ conversion. *Dalt. Trans.* **2020**, *49*, 16608–16616. [CrossRef] [PubMed]

31. Ahlquist, M.S.G. Iridium Catalyzed Hydrogenation of CO₂ under Basic Conditions—Mechanistic Insight from Theory. *J. Mol. Catal. A Chem.* **2010**, *324*, 3–8. [CrossRef]

32. Yang, X. Hydrogenation of Carbon Dioxide Catalyzed by PNP Pincer Iridium, Iron, and Cobalt Complexes: A Computational Design of Base Metal Catalysts. *ACS Catal.* **2011**, *1*, 849–854. [CrossRef]

33. Hou, C.; Jiang, J.; Zhang, S.; Wang, G.; Zhang, Z.; Ke, Z.; Zhao, C. Hydrogenation of Carbon Dioxide Using Half-Sandwich Cobalt, Rhodium, and Iridium Complexes: DFT Study on the Mechanism and Metal Effect. *ACS Catal.* **2014**, *4*, 2990–2997. [CrossRef]

34. Jeletic, M.S.; Helm, M.L.; Hulley, E.B.; Mock, M.T.; Appel, A.M.; Linehan, J.C. A Cobalt Hydride Catalyst for the Hydrogenation of CO₂: Pathways for Catalysis and Deactivation. *ACS Catal.* **2014**, *4*, 3755–3762. [CrossRef]

35. Ogo, S.; Kabe, R.; Hayashi, H.; Harada, R.; Fukuzumi, S. Mechanistic Investigation of CO_2 Hydrogenation by Ru(II) and Ir(III) Aqua Complexes under Acidic Conditions: Two Catalytic Systems Differing in the Nature of the Rate Determining Step. *Dalt. Trans.* **2006**, *39*, 4657–4663. [CrossRef] [PubMed]

36. Mondal, B.; Neese, F.; Ye, S. Control in the Rate-Determining Step Provides a Promising Strategy to Develop New Catalysts for CO_2 Hydrogenation: A Local Pair Natural Orbital Coupled Cluster Theory Study. *Inorg. Chem.* **2015**, *54*, 7192–7198. [CrossRef] [PubMed]

37. Mondal, B.; Neese, F.; Ye, S. Toward Rational Design of 3d Transition Metal Catalysts for CO_2 Hydrogenation Based on Insights into Hydricity-Controlled Rate-Determining Steps. *Inorg. Chem.* **2016**, *55*, 5438–5444. [CrossRef] [PubMed]

38. Erken, C.; Kaithal, A.; Sen, S.; Weyhermüller, T.; Hölscher, M.; Werlé, C.; Leitner, W. Manganese-Catalyzed Hydroboration of Carbon Dioxide and Other Challenging Carbonyl Groups. *Nat. Commun.* **2018**, *9*, 4521. [CrossRef] [PubMed]

39. Zhang, L.; Pu, M.; Lei, M. Hydrogenation of CO_2 to Methanol Catalyzed by a Manganese Pincer Complex: Insights into the Mechanism and Solvent Effect. *Dalt. Trans.* **2021**, *50*, 7348–7355. [CrossRef] [PubMed]

40. Zhang, Y.; MacIntosh, A.D.; Wong, J.L.; Bielinski, E.A.; Williard, P.G.; Mercado, B.Q.; Hazari, N.; Bernskoetter, W.H. Iron Catalyzed CO_2 Hydrogenation to Formate Enhanced by Lewis Acid Co-Catalysts. *Chem. Sci.* **2015**, *6*, 4291–4299. [CrossRef] [PubMed]

41. Lane, E.M.; Zhang, Y.; Hazari, N.; Bernskoetter, W.H. Sequential Hydrogenation of CO_2 to Methanol Using a Pincer Iron Catalyst. *Organometallics* **2019**, *38*, 3084–3091. [CrossRef]

42. Rong, H.; Zhang, Y.; Ai, X.; Li, W.; Cao, F.; Li, L. Theoretical Study on the Hydrogenolysis of Polyurethanes to Improve the Catalytic Activities. *Inorg. Chem.* **2022**, *61*, 14662–14672. [CrossRef]

43. Frisch, M.J.; Trucks, G.W.; Schlegel, H.B.; Scuseria, G.E.; Robb, M.A.; Cheeseman, J.R.; Scalmani, G.; Barone, V.; Petersson, G.A.; Nakatsuji, H.; et al. *Gaussian 16, Revision C.01*; Gaussian, Inc.: Wallingford, CT, USA, 2016.

44. Muckerman, J.T.; Achord, P.; Creutz, C.; Polyansky, D.E.; Fujita, E. Calculation of Thermodynamic Hydricities and the Design of Hydride Donors for CO_2 Reduction. *Proc. Natl. Acad. Sci. USA* **2012**, *109*, 15657–15662. [CrossRef]

45. Zhang, X.M.; Bruno, J.W.; Enyinnaya, E. Hydride Affinities of Arylcarbenium Ions and Iminium Ions in Dimethyl Sulfoxide and Acetonitrile. *J. Org. Chem.* **1998**, *63*, 4671–4678. [CrossRef]

46. Ellis, W.W.; Raebiger, J.W.; Curtis, C.J.; Bruno, J.W.; DuBois, D.L. Hydricities of BzNADH, $C_5H_5Mo(PMe_3)(CO)_2H$, and $C_5Me_5Mo(PMe_3)(CO)_2H$ in Acetonitrile. *J. Am. Chem. Soc.* **2004**, *126*, 2738–2743. [CrossRef] [PubMed]

47. Curtis, C.J.; Miedaner, A.; Ellis, W.W.; DuBois, D.L. Measurement of the Hydride Donor Abilities of $[HM(Diphosphine)_2]^+$ Complexes (M = Ni, Pt) by Heterolytic Activation of Hydrogen. *J. Am. Chem. Soc.* **2002**, *124*, 1918–1925. [CrossRef] [PubMed]

48. Fong, H.; Peters, J.C. Hydricity of an Fe-H Species and Catalytic CO_2 Hydrogenation. *Inorg. Chem.* **2015**, *54*, 5124–5135. [CrossRef]

49. Fang, H.; Jing, H.; Ge, H.; Brothers, P.J.; Fu, X.; Ye, S. The Mechanism of E-H (E = N, O) Bond Activation by a Germanium Corrole Complex: A Combined Experimental and Computational Study. *J. Am. Chem. Soc.* **2015**, *137*, 7122–7127. [CrossRef] [PubMed]